The Plant Journal (2005) **44**, 516–529 doi: 10.1111/j.1365-313X.2005.02545.x

Arabidopsis thaliana subcellular responses to compatible *Erysiphe cichoracearum* infections

Serry Koh[1], Aurélie André[1,†], Herb Edwards[2], David Ehrhardt[1] and Shauna Somerville[1,*]
[1]*Carnegie Institution, Department of Plant Biology, 260 Panama St, Stanford, CA 93405, USA, and*
[2]*Department of Biological Sciences, Western Illinois University, Macomb, IL 61455, USA*

Received 24 May 2005; revised 3 August 2005; accepted 8 August 2005.
[*]For correspondence (fax +1 650 325 6857; e-mail ssomerville@stanford.edu).
[†]Present address: Unibioscreen, 40 Ave. J. Wybran, 1070 Brussels, Belgium.

Summary

Subcellular events of *Erysiphe cichoracearum* infections of epidermal cells were visualized in living tissues of Arabidopsis plants carrying various green fluorescent protein (GFP)-tagged organelles via laser scanning confocal microscopy. Early in the infection sequence, cytoplasm and organelles moved towards penetration sites and accumulated near penetration pegs. Peroxisomes appeared to accumulate preferentially relative to the cytoplasm at penetration sites. Another early event, which preceded haustorium formation, was the aggregation of some GFP-tagged plasma membrane marker proteins into rings around penetration sites, which extended across cell-wall boundaries into neighboring cells. This feature localized to sites where papillae were deposited. The extrahaustorial membrane (EHM) encases the fungal feeding structure, the haustorium, separating it from the host cytoplasm. Eight plasma membrane markers were excluded from the EHM and remained in a collar-like formation around the haustorial neck. These observations support the suggestions that the EHM is a unique, specialized membrane and is different from the plasma membrane. Our results suggested two possibilities for the origin of the EHM: invagination of the plasma membrane coupled with membrane differentiation; or *de novo* synthesis of the EHM by targeted vesicle trafficking.

Keywords: green fluorescent protein, haustorial complex, laser scanning confocal microscopy, organelle, plant–pathogen interactions, powdery mildew.

Introduction

The powdery mildews are obligate biotrophic fungi, and are one of the most economically important groups of plant pathogens (Agrios, 1997). As a family, the powdery mildews infect a broad range of plant species including barley, wheat, pea, apple, sugar beet and grape (Braun, 1987). Three species are known to cause disease on Arabidopsis: *Erysiphe cichoracearum* (=*Golovinomyces cichoracearum*) (Adam *et al.*, 1999), *Erysiphe orontii* (=*Golovinomyces orontii*) (Plotnikova *et al.*, 1998), and *Erysiphe cruciferarum* (Adam *et al.*, 1999).

Because infections are limited to the plant surface and epidermis, powdery mildew infections have been studied in some detail microscopically (for recent reviews see Bushnell, 2002; Green *et al.*, 2002). Many of these studies focused on the early stages of infections of pea by *Erysiphe pisi* (Bushnell and Gay, 1978; Gil and Gay, 1977; Manners and Gay, 1977, 1983) and of barley by *Blumeria graminis* f. sp. *hordei* (Bracker, 1968; Bushnell and Gay, 1978; Nicholson and Kunoh, 1994). The earliest event is the release of an exudate, containing cutinases and other proteinaceous compounds, by the conidia of *B. graminis* f. sp. *hordei* on contact with a hydrophobic surface (Nicholson *et al.*, 1988; Pascholati *et al.*, 1992). Within 24 h after inoculation (hai), powdery mildew conidia germinate, develop appressoria, form penetration pegs from appressoria, penetrate the host outer epidermal cuticle and cell wall, and establish haustorial complexes within epidermal cells (Figure 1). Successful establishment of the haustorial complex allows the pathogen to draw water, minerals and nutrients from the host cell and supports continued hyphal growth on the leaf surface.

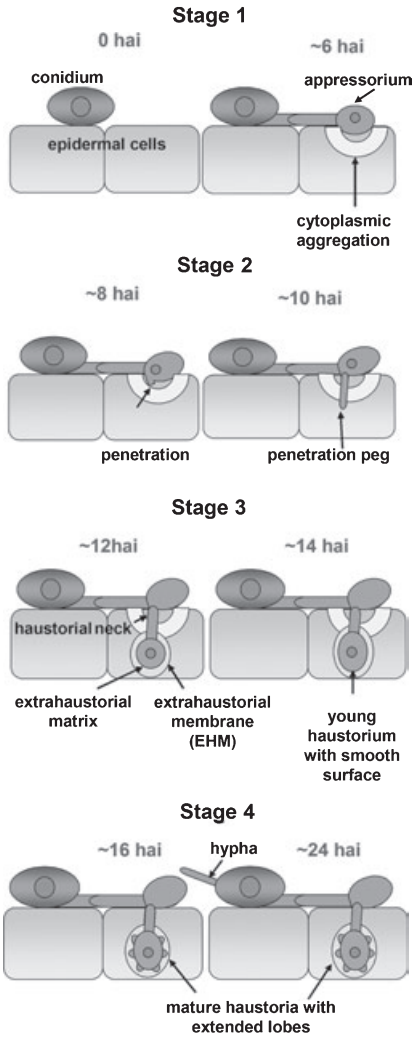

Figure 1. Infection sequence of *Erysiphe cichoracearum* UCSC1 on a susceptible Arabidopsis host, Col-0, up to 24 hai (see text for additional description of each stage of infection).

The haustorial complex, which consists of the fungal haustorium, the extrahaustorial matrix and the host extrahaustorial membrane (EHM), develops within 12–18 hai. The fungal haustorium is a sac-like structure of fungal origin, with lobes of varying size depending on the powdery mildew species. Although it has long been assumed that haustoria are feeding structures, the identification of transporters (e.g. hexose transporter, amino acid permease) in the plasma membrane of *Uromyces fabae* haustoria (Hahn *et al.*, 1997; Voegele *et al.*, 2001), and the demonstration that glucose appears to be transported from wheat to the wheat powdery mildew (Sutton *et al.*, 1999), lend experimental support to this idea. The haustorium is separated from the cytoplasm of the infected epidermal cell by the EHM and the gel-like amorphous extrahaustorial matrix. The EHM is thought to be host-derived, although the pathogen may contribute components to this specialized membrane, and the extrahaustorial matrix may be of both fungal and host origin. Two haustorial neckbands appear to seal the EHM to the haustorial neck and limit access to the extrahaustorial matrix from the apoplast (Bracker, 1968; Bushnell, 1972; Bushnell and Gay, 1978; Gil and Gay, 1977; Manners and Gay, 1977, 1982). The EHM differs from the host plasma membrane in both cytological and biochemical properties (Bracker, 1968; Bushnell and Gay, 1978). In powdery mildew-infected pea leaves, the EHM appeared thicker and more convoluted than the plant plasma membrane in transmission electron micrographs (TEM). Also, the EHM lacks typical plasma membrane components, including intramembrane particles detected by freeze-fraction methods and the biochemical markers ATPase and α-glycerophosphatase (Gil and Gay, 1977; Manners and Gay, 1983; Spencer-Phillips and Gay, 1981). Using monoclonal antibodies, Green and colleagues identified epitopes that occurred in the plasma membrane and/or the EHM (Green *et al.*, 1995; Mackie *et al.*, 1993; Roberts *et al.*, 1993). Among their collection of monoclonal antibodies, one recognized an epitope that occurred only in newly developed EHM, while a second bound to an epitope that appeared only in mature EHM [5–7 days after inoculation (dai)], suggesting that EHM composition changes over time (Mackie *et al.*, 1993; Roberts *et al.*, 1993). Although host nutrients and water must cross the EHM to reach the fungal haustorium, little is known about either the specific functional capabilities of the EHM or its origin.

A number of cellular host responses to powdery mildew infections have been observed by Nomarski and/or fluorescence light microscopy. Among the earliest is the accumulation of cytoplasmic content in aggregates at the site of penetration, which is thought to be mediated by changes in cytoplasmic streaming (Bracker, 1968; Kobayashi *et al.*, 1995). Bushnell and colleagues showed that these cytoplasmic aggregates formed under appressoria prior to the appearance of papillae and haustoria in *B. graminis* f. sp. *hordei*-infected barley coleoptile cells (Bushnell and Bergquist, 1975; Bushnell and Zeyen, 1976). The cytoplasmic aggregates formed quickly and generally then dispersed within about 3.5–5 h of their appearance (Bushnell and Zeyen, 1976; Clark *et al.*, 1995; Koga *et al.*, 1990). When an appressorium formed near the junction of two cells, cytoplasmic aggregates were observed in the cell adjacent to the attacked cell. These cytoplasmic aggregates contained numerous organelles and vesicles characteristic of active cells, suggesting they may participate in papillae deposition and host cell-wall modifications that occur in the same time frame (Bushnell and Zeyen, 1976). Papillae, callose-rich cell-wall appositions, and halo-like formations of autofluorescent materials are deposited in the host cell wall at penetration sites (Mendgen *et al.*, 1995; Zeyen and Bushnell, 1979; Zeyen *et al.*, 2002). Cytoplasmic aggregates, papillae and cell-wall halos form in compatible, incompatible and non-host interactions, and in response to the primary germ tubes of cereal

powdery mildews, suggesting that such responses are generalized host responses to attempted penetration (Bushnell and Bergquist, 1975; Clark *et al.*, 1995; Koga *et al.*, 1990).

Many of these cytological responses, such as the appearance of cytoplasmic aggregates, apparent changes in cytoplasmic streaming, targeted movement of vesicles to penetration sites and the formation of papillae, are thought to be dependent on the cytoskeleton. In a study of live cell imaging of oomycete infections of Arabidopsis with either green fluorescent protein (GFP)-tagged tubulin or GFP-tagged talin, the actin-binding protein, rearrangements of actin microfilaments but not microtubules were observed in both compatible and incompatible interactions between Arabidopsis and the obligate biotrophic downy mildew (Takemoto *et al.*, 2003). One study reported that inhibitors of actin microfilaments partially reduced susceptibility to a biotrophic rust fungus, which would be consistent with a role for actin rearrangements in compatible interactions (Škalamera and Heath, 1998).

The broad goal of this study was to monitor in detail the early events of powdery mildew infections of susceptible Arabidopsis hosts during the first 24 hai. Previous studies showed that formation of cytoplasmic aggregates was a rapid response to fungal attack (Bushnell and Zeyen, 1976; Clark *et al.*, 1995; Koga *et al.*, 1990). We wished to know whether specific organelles accumulated preferentially at penetration sites. A second goal was to ascertain whether any of the available GFP-tagged markers could be used to study the formation of the EHM, a membrane critical to successful fungal infections. The availability of Arabidopsis lines with different organelles tagged with GFP, yellow fluorescent protein (YFP), or cyan fluorescent protein (CFP), together with improved visualization by laser scanning confocal microscopy (LSCM), allowed us to determine the subcellular spatial distribution of host organelles relative to penetration sites, and to observe changes in the distribution of the plasma membrane as haustorial complexes developed (Cutler *et al.*, 2000; Ehrhardt, 2003). We show that the EHM is not labeled by GFP-tagged plasma membrane proteins, indicating that it is a unique membrane different from the host plasma membrane. We suggest two alternative models for EHM synthesis. Furthermore, the cytoplasm and all organelle types appeared to move to penetration sites and aggregate near the haustorial neck, consistent with a concerted response of the host to fungal attack.

Results

Infection stages during the E. cichoracearum*–Arabidopsis interaction*

To visualize the development of haustoria within epidermal cells, as well as other fungal structures, infected Arabidopsis leaves were stained with trypan blue and observed by bright-field light microscopy. By 24 hai, >80% of germinated conidia had formed appressoria and haustoria (data not shown). Generally, a hypha had also emerged from the conidium opposite the appressorial germ tube, suggesting the haustorium was functional and nutrient transfer to the fungus was successful. At 2 dai, three elongated fungal hyphae had formed from a single conidium. Subsequently, these hyphae extended across the leaf surface. Conidiophores started to form at 5 dai, and by 7 dai the leaves had a powdery appearance which was easily detected by the naked eye.

As we were interested in the host subcellular processes that accompany haustorial complex formation, we focused our studies on the first 24 hai, a period that encompasses the formation of the first haustorium of a developing colony. Due to non-synchronous conidium germination, a wide range of infection stages were observed at a single sampling time. To aid comparisons among different infections of the various Arabidopsis lines, the infection sequence was divided into four stages (Figure 1) based on the presence of host and fungal structures. In stage 1 (0–6 hai), the conidium had germinated and the germ tube with its appressorium had developed, but no penetration into the plant cell was observed. Cytoplasmic aggregates often appeared in the host epidermal cell underneath appressoria at this stage. Stage 2 (6–10 hai) was defined as the period in which the appressorium developed a long, thin penetration peg, which subsequently penetrated the epidermal cell. No haustorium had developed by this stage. Stage 3 (10–14 hai) was defined as the period in which the haustorium first formed at the end of the penetration peg as a swollen, elongated sac with a smooth surface. At this stage, nuclear migration from the hypha on the leaf surface into the haustorium was complete, and a septum separated the body from the neck. Stage 4 (14–24 hai) was the last stage of the early infection process, and was characterized by the occurrence of a haustorium with distinct lobes emanating from the body. By stage 4 a hypha had emerged from the conidium at the side opposite the appressorial germ tube. This sequence of events resembled the infection sequences for other powdery mildews, with the exception that the cereal powdery mildews produce a vestigial primary germ tube prior to an appressorial germ tube.

Plasma membrane changes following inoculation with powdery mildew

In uninfected epidermal leaf cells, the plasma membrane appeared as a continuous smooth line on the cell periphery, inside the cell wall, as visualized with all eight plasma membrane marker lines (Figure 2a; Table 1). During stage 1, no distinguishable fungal structures developed within the plant cell, and no invagination or vesiculation of the

plasma membrane was apparent in the eight GFP-plasma membrane marker lines in infected plant cells (data not shown).

One of the earliest events observed was the formation of a large ring of GFP signal with several plasma membrane marker lines (37-26, 29-1 and D41) prior to fungal penetration into the host epidermal cell (Figure 2i). This structure was observed at 21–70% of penetration sites, depending on the marker line, in stages 1 and 2 (Table 2), and the frequency of occurrence diminished over time. The diameter of the largest, outer ring (13–38 μm, $n = 25$) corresponded in size roughly to the diameter of the papilla (18–26 μm, $n = 12$) (Figure 2j). Often a series of one or more smaller rings was observed, arranged in a concentric fashion inside the largest ring (Figure 2i). As reported for the cytoplasmic aggregates and autofluorescent halos, the rings could cross cell boundaries (Figure 2i).

In stage 2, many small, vesicle-like structures were detected near penetration sites (Figure 2b). Pouch-like structures formed near long, thin penetration pegs during stages 2–3, prior to the formation of haustorial bodies (Figure 2c–e). These pouch-like structures did not persist. By stages 3 and 4, only a collar of plasma membrane around the haustorial neck was observed (Figure 2f–h).

Beginning in stage 2 and persisting through stage 4, a double-annulus structure was observed using GFP-tagged plasma membrane proteins (Figure 2k). This annulus featured two concentric rings and was much smaller in diameter than the ring-like aggregations of plasma mem-

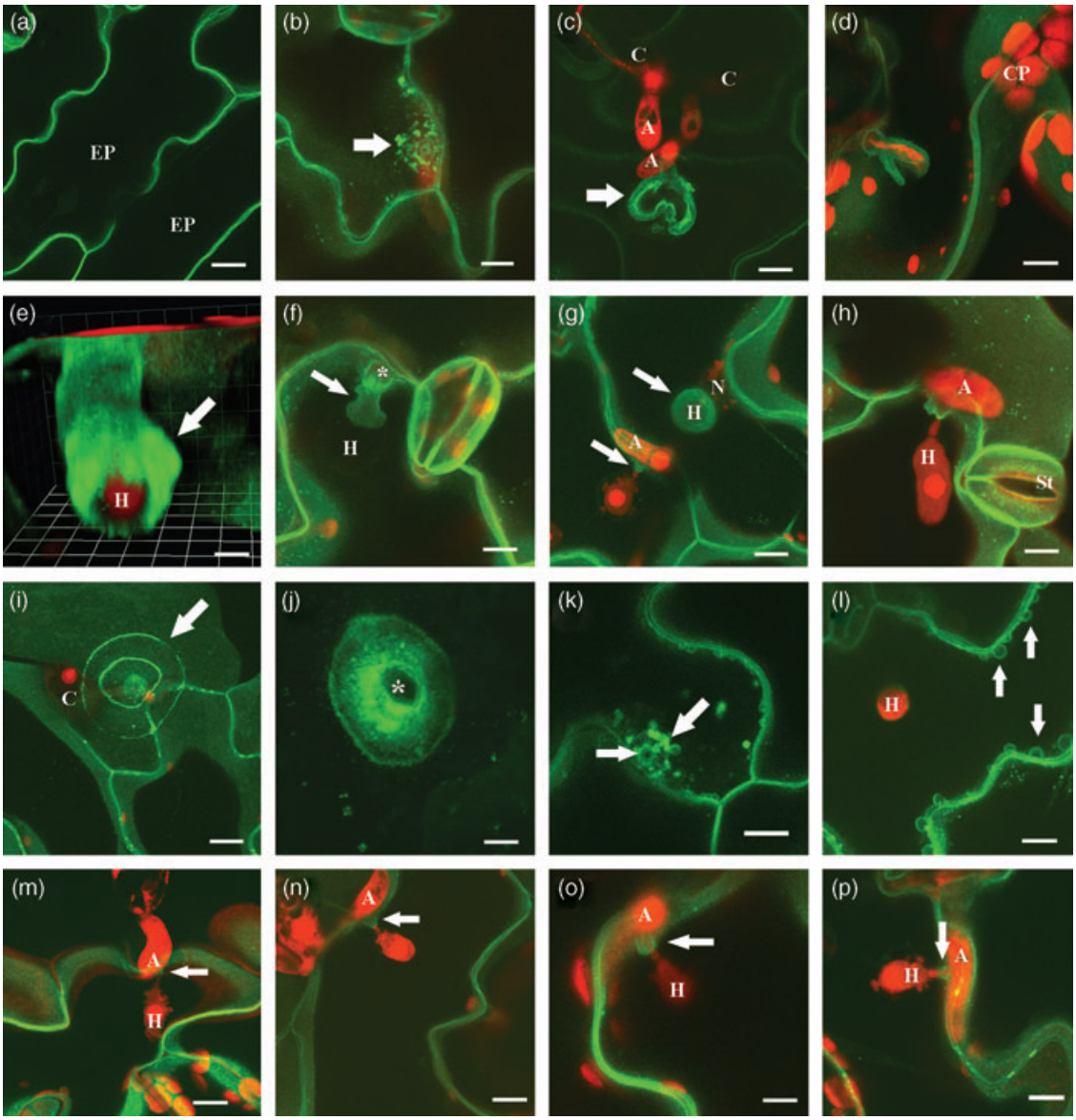

brane proteins observed in stage 1 (cf. Figure 2i,k). From these confocal observations and by comparison with the TEM, we believe that the inner ring of the annulus abuts the haustorial neck region.

Very active plasma membrane dynamics were visible by LSCM in infected host epidermal cells. During stages 2–3, bubble-like vesicular structures were observed adjacent to the plasma membrane both at sites near and distal to the penetration site (Figure 2l). Smaller, vesicular structures were also found at the boundary of the double annulus that encircled the haustorial neck (Figure 2k).

Several plasma membrane proteins are missing from the extrahaustorial membrane

In stages 3 and 4, when haustorial complexes were present, no GFP labeling of the EHM was observed with any of the eight plasma membrane marker proteins. Rather, the plasma membrane was restricted to a collar-like structure encasing the upper part of the haustorial neck region. This labeling pattern was easiest to observe in one of the strongest GFP-expressing plasma membrane marker lines, 37-26 (Figure 2a–h). Lines Q8, Leez, 29-1 and D41 also showed clear labeling of the plasma membrane, but not of the EHM (Figure 2m–p). Three additional plasma membrane-tagged proteins, GFP-SIMIP, GFP-PIP1b and Bri1-GFP, also formed a collar around the haustorial neck, but were weakly expressed in mature rosette leaves and thus difficult to image (data not presented). The GFP-tagged marker proteins represent a diverse array of plasma membrane proteins. A majority of the proteins are tagged with GFP at the N-terminus; however, the BRI1 protein is tagged with GFP at the C-terminus. Given both the number of protein markers tested and the diversity of their functions, it seems unlikely that the absence of labeling of the EHM is an anomaly. Thus our observations are consistent with the idea that the EHM has characteristics distinct from the plasma membrane.

Erysiphe cichoracearum *haustoria*

With LSCM, small lobes extending from the body of mature haustoria of *E. cichoracearum* were observed (Figure 2g,m,p). These haustorial lobes were also visible by TEM (Figure 3a,b) and in isolated haustorial complexes (Figure 3c,d). The lobes appeared to develop last in the mid-zone of the haustorium, and were more prominent near the neck region and at the base of the haustorium. Previous TEM studies reported that the *E. pisi* haustorium developed lobes when mature (Gil and Gay, 1977). Most powdery mildew haustoria, with the exception of *B. graminis* haustoria with their extended finger-like lobes, are round to pear-

Figure 2. Host plasma membrane dynamics during *Erysiphe cichoracearum* infections.
(a–i) and (k–p) green fluorescent protein (GFP)-tagged plasma membrane marker lines were infected with *E. cichoracearum* (except as noted), stained with propidium iodide to highlight fungal structures and visualized by LSCM. A, appressorium; CP, chloroplast; C, conidium; EP, epidermal cell; H, haustorium; N, nucleus; St, stomate.
(a) Visualization of the plasma membrane with GFP-LTI6a in uninfected leaf epidermal cells. Bar = 22.7 μm.
(b) Aggregations of vesicles (arrow), labeled with a GFP-tagged plasma membrane protein (GFP-LTI6a), at the infection site in early stage 1 infections. Bar = 9.4 μm.
(c) Pouch-like structures (arrow) develop from the plasma membrane where the future haustorium will form in early stage 2 infections. Bar = 14.5 μm.
(d) Plasma membrane (arrow) encompasses the penetration peg and immature haustorial complex at late stage 2 (37-26 marker line). Chloroplasts from underlying mesophyll cells also fluoresce in the red channel. Bar = 6.3 μm.
(e) Extended plasma membrane (arrow) encompasses a developing young haustorial complex in stage 3 (37-26 marker line). Z-series of 40 images were 3D volume rendered using VOLOCITY image software. Bar = 4.2 μm.
(f) The plasma membrane encases the neck region of the haustorial complex (arrow). (stage 3, 37-26 marker line). *, Penetration site. Bar = 4.7 μm.
(g) Adjacent cells with two different stages of developing haustoria (arrows; left, stage 4; right, early stage 3) show that the GFP-labeled plasma membrane encasing the upper part of the haustorial complex was more extensive for younger haustorial complexes (right, stage 3) and was restricted to a collar around the distal neck region as the haustorial complex matured (left, stage 4) (37-26 marker line). Bar = 14.5 μm.
(h) The GFP-LTI6a plasma membrane marker protein remained around the haustorial complex neck area and did not label the EHM in this stage 3 infection (37-26 marker line). Bar = 9.5 μm.
(i) The GFP-tagged plasma membrane AtVamp3 marker aggregated into a multi-ring structure at the penetration attempt site at stage 1. The outer ring crossed the cell-wall boundary into an adjacent cell. Bar = 12.3 μm.
(j) Callose, which was visualized with a monoclonal anti-callose antibody and an Alexa 488-labeled secondary antibody, is a major component of papillae, plant cell-wall appositions that form at penetration sites (*). Bar = 5.2 μm.
(k) Concentric rings of fluorescence (double annulus) at the infection site. Arrows point to the inner and outer annuli. Numerous vesicles aggregate at the outer ring of the double annulus suggestive of active membrane exocytosis or endocytosis GFP-LTI6b plasma membrane marker). Bar = 5.9 μm.
(l) Bubble-like vesicles (arrows) labeled with the plasma membrane marker GFP-PIP2a are observed distal to penetration sites at stage 3, suggesting that additions to the plasma membrane are not confined to the site of fungal penetration during haustorium development. Bar = 6.8 μm.
(m) GFP-tagged plasma membrane marker line Q8 visualized at stage 4. Arrow points to the collar of plasma membrane surrounding the neck of the haustorial complex. Bar = 9.6 μm.
(n) GFP-tagged plasma membrane marker line Leez visualized at stage 3. Arrow points to the collar of plasma membrane surrounding the neck of the haustorial complex. Bar = 10.3 μm.
(o) GFP-tagged plasma membrane marker line 29-1 visualized at stage 4. Arrow points to the collar of plasma membrane surrounding the neck of the haustorial complex. Bar = 4.9 μm.
(p) GFP-tagged plasma membrane marker line D41 visualized at stage 4. Arrow points to the collar of plasma membrane surrounding the neck of the haustorial complex. Bar = 7 μm.

Table 1 Green fluorescent protein (GFP), yellow fluorescent protein (YFP) and cyan fluorescent protein (CFP)marker lines

Target organelle	Line[a]	Protein	Protein function	Source[b]
Plasma membrane	37-26	GFP-LTI6a	Low temperature-induced protein	Cutler *et al.* (2000)
	29-1	GFP-LTI6b	Low temperature-induced protein	Cutler *et al.* (2000)
	Q8	GFP-PIP2a	Aquaporin	Cutler *et al.* (2000)
	D41	GFP-AtVamp3	Truncated syntaxin	Cutler *et al.* (2000)
	PM	GFP-SIMIP	Aquaporin	Cutler *et al.* (2000)
	160698D (Q7)	GFP-PIP1b	Aquaporin	Cutler *et al.* (2000)
	Leez	GFP-Tuba6A	Out-of-frame fusion protein	Cutler *et al.* (2000)
	Bri1	BRI1-GFP	Brassinosteriod receptor	Friedrichsen *et al.* (2000)
Peroxisome	A5	GFP-Tetrafunctional protein	Luminal protein for β-oxidation	Cutler *et al.* (2000)
	150698I (C4)	GFP-γ-TIP	Out of frame γ-TIP	Cutler *et al.* (2000)
	A5Y + ECAD[c]	EYFP-Tetrafunctional protein + ECFP	Luminal protein for β-oxidation + cytoplasmic ECFP	This study[b]
Golgi bodies	Dscs[d]	GFP-Novel protein	Golgi body protein	Cutler *et al.* (2000)
Endoplasmic reticulum	Q4 (SNO)[e]	GFP-Novel protein	ER protein, with lysine rich C-terminus	Cutler *et al.* (2000)
Vacuole	Q5 (VacM)	GFP-δ-TIP	Tonoplast aquaporin	Cutler *et al.* (2000)
	Q5Y + ECAD[c]	EYFP- δ-TIP + ECFP	Tonoplast aquaporin + cytoplasmic ECFP	This study[b]
Mitochondria-like structures	Q10	GFP-Novel protein	Glycine-rich protein 32	Cutler *et al.* (2000)
Cytoplasm	EGAD	EGFP	Cytoplasmic green fluorescent protein	Cutler *et al.* (2000)
	ECAD[f]	ECFP	Cytoplasmic cyan fluorescent protein	Miyawaki *et al.* (1997)

[a]Alternative names in parentheses.
[b]More information about the markers (except BRI-GFP) can be found at http://deepgreen.stanford.edu
[c]Double marker lines were created by genetic crossing.
[d]Dscs is a novel protein that co-localizes with the Golgi marker AtFT1 (fucosyl transferase 1) (unpublished data).
[e]Q4 is a fusion to a novel protein that localizes to the ER. It contains a short sequence rich in lysine which may act as an ER retention signal.
[f]pECAD is a plasmid that expresses the ECFP gene from a 35S promoter. It is a derivative of the pEGAD plasmid created by J. Griffits and D. Ehrhardt (http://deepgreen.stanford.edu). pECAD was introduced into Col-0 to create line ECAD.

Table 2 Occurrence of rings of plasma membrane markers upon infection with *Erysiphe cichoracearum*

Line	Occurrences of a large ring
D41	37[a]/53[b] (70%[c])
37-26	3/14 (21%)
29-1	3/14 (21%)
Total	43/81 (53%)

[a]Number of penetration sites with one or more large rings in stage 1 or 2 infections.
[b]Total number of penetration sites observed.
[c]Percentage of penetration sites with large rings.

shaped with compact lobes of varying size and number (Braun, 1987) and *E. cichoracearum* fits this morphological pattern.

TEM images of *E. cichoracearum*-infected Arabidopsis leaves showed the presence of a haustorial neck band, an electron-dense area along the haustorial neck (Figure 3b). The neck band is thought to form a seal between the plasma membrane or EHM and the fungal cell wall (Bracker, 1968; Bushnell, 1972; Bushnell and Gay, 1978; Gil and Gay, 1977; Manners and Gay, 1977, 1982). The number of neck bands in *E. cichoracearum* was unclear from these images. *Erysiphe pisi* and *B. graminis* f. sp. *hordei* have at least two haustorial neckbands, isolating the haustorial complex from the plant apoplastic space (Gil and Gay, 1977). The origin of these haustorial neckbands is unknown. In isolated haustorial complexes, the EHM appeared to be connected to the haustorium only in the neck region above the fungal septum separating the haustorium from the penetration peg (Figure 3c,d). This conclusion was supported by the observation that isolated haustoria either had an intact EHM or completely lacked the EHM. No haustoria with fragments of adhering EHM were recovered (data not shown), as might be expected if the EHM were attached to haustoria at multiple contact points. Comparison between *in vivo* haustorial complexes visualized within an infected cell (Figure 3e) and isolated haustorial complexes (Figure 3c,d,f) suggested that the plasma membrane collar encircling the haustorial neck and the haustorial neckbands were coincident.

Aggregation of organelles at penetration sites

Using cytoplasmic forms of GFP (EGAD, Table 1) or CFP (ECAD, Table 1), we were able to observe movement of cytoplasm toward penetration sites in stages 1–2 during the infection process (Figure 4a). In addition, the movements of the various host organelle types in powdery mildew-attacked cells were compared individually in infected and

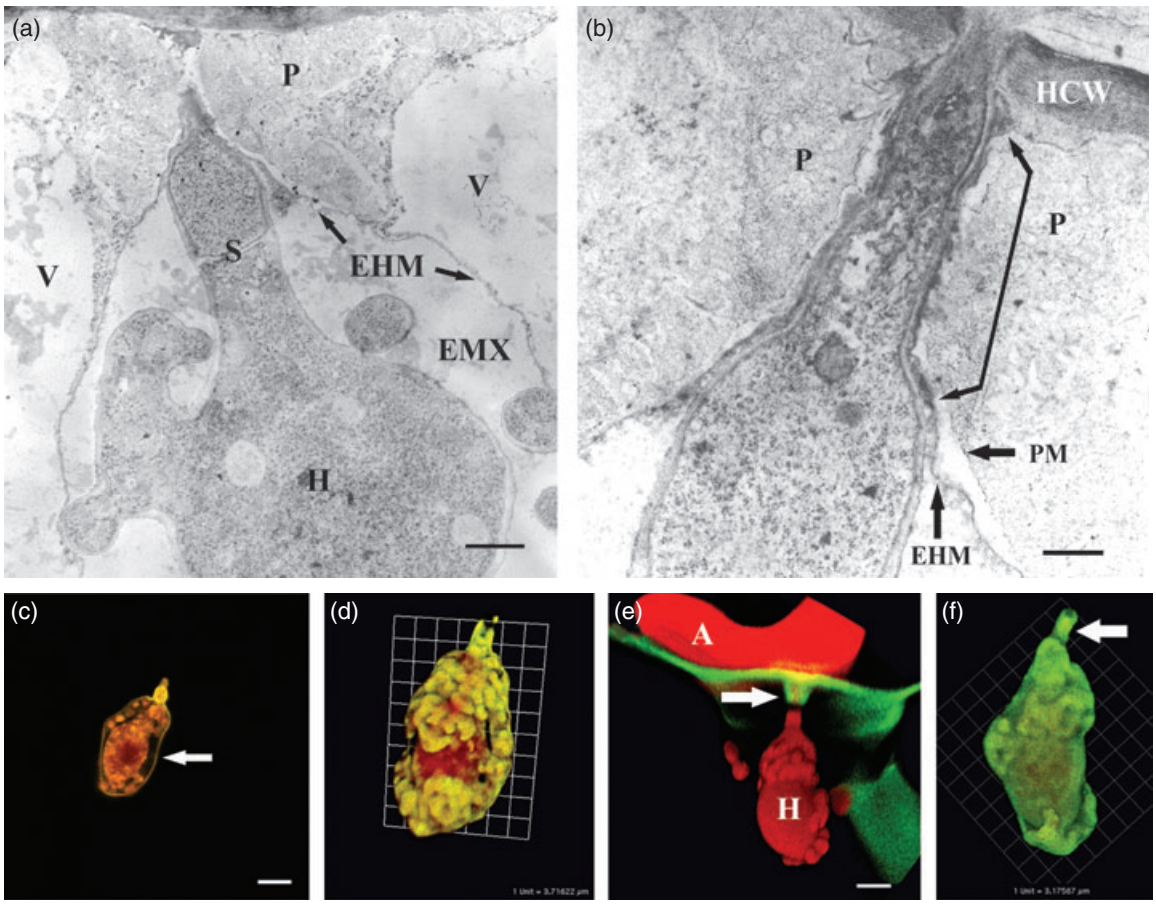

Figure 3. Morphology of the *Erysiphe cichoracearum* haustorium and haustorial complex.
Transmission electron microscopy (a, b) and LSCM (e) of *in vivo* haustorial complexes from *E. cichoracearum*-infected Arabidopsis Col-0; and LSCM of isolated haustorial complexes from *E. cichoracearum*-infected squash (c, d, f). A, appressorium; EHM, extrahaustorial membrane; EMX, extrahaustorial matrix; H, haustorium; HC, host cytoplasm; HCW, host cell wall; P, papilla; S, fungal septum; V, vacuole.
(a) A mature haustorium at stage 4 with lobe-like extensions around the haustorium surface. A papilla was present and host cytoplasm occurred as a thin layer in between the EHM and vacuole. Bar = 1.4 μm.
(b) The haustorial neck area showed an electron-dense area (arrows) suggesting the presence of the haustorial neckband. Bar = 0.6 μm.
(c) An isolated mature haustorial complex with an intact EHM (arrow). The haustorium has lobe-like extensions. Sample stained with propidium iodide and FM 1–43, and visualized with LSCM. Bar = 8.4 μm.
(d) A 3D volume-rendered isolated haustorial complex. Elaborate lobe-like structures were shown around the mature haustorium. Sample stained with FM 1–43 and propidium iodide. Grid unit = 3.71 μm.
(e) A 3D volume-rendered *in vivo* haustorial complex. GFP-tagged plasma membrane marker (37-26) forms a collar (arrow) around the haustorial neck. Fungal structures are stained with propidium iodide. Image was generated from a Z-series of 19 scans (0.5 μm per scan). Bar = 4.5 μm.
(f) A 3D volume-rendered isolated haustorial complex. The EHM followed the contours of the haustorium lobes and appeared tightly joined at the haustorial neckband region (arrow). Sample stained with FM 1–43 and propidium iodide. Grid unit = 3.17 μm.

uninfected cells, using time-lapse LSCM images of a single focal plane that spanned a period of 300 sec (60 scans at 5-sec intervals) (Figure 4).

Nucleus and endoplasmic reticulum. The nucleus of an infected host epidermal cell appeared roughly twice as large as that of an uninfected cell. In previous studies, this infection-associated increase in nuclear volume was proposed to be due to active transcription and endo-reduplication (Baluška *et al.*, 1995). In addition to increased size, the nucleus moved from its typical position at the bottom of the epidermal cell, adjacent to the underlying mesophyll cells, closer to the penetration site and developing haustorial complex during the early infection stages (Figure 4b), as has been observed in compatible cowpea–cowpea rust interactions (Škalamera and Heath, 1998). Movement of the nucleus and of the ER occurred in a similar time frame (Figure 4b). The ER appeared as a net-like structure, closely enveloping the developing haustorial complex with the majority of the ER in this region aggregated at the haustorial neck region (Figure 4c).

Peroxisomes, mitochondria and Golgi bodies. As shown in Figure 4(d–f), large numbers of peroxisomes had already

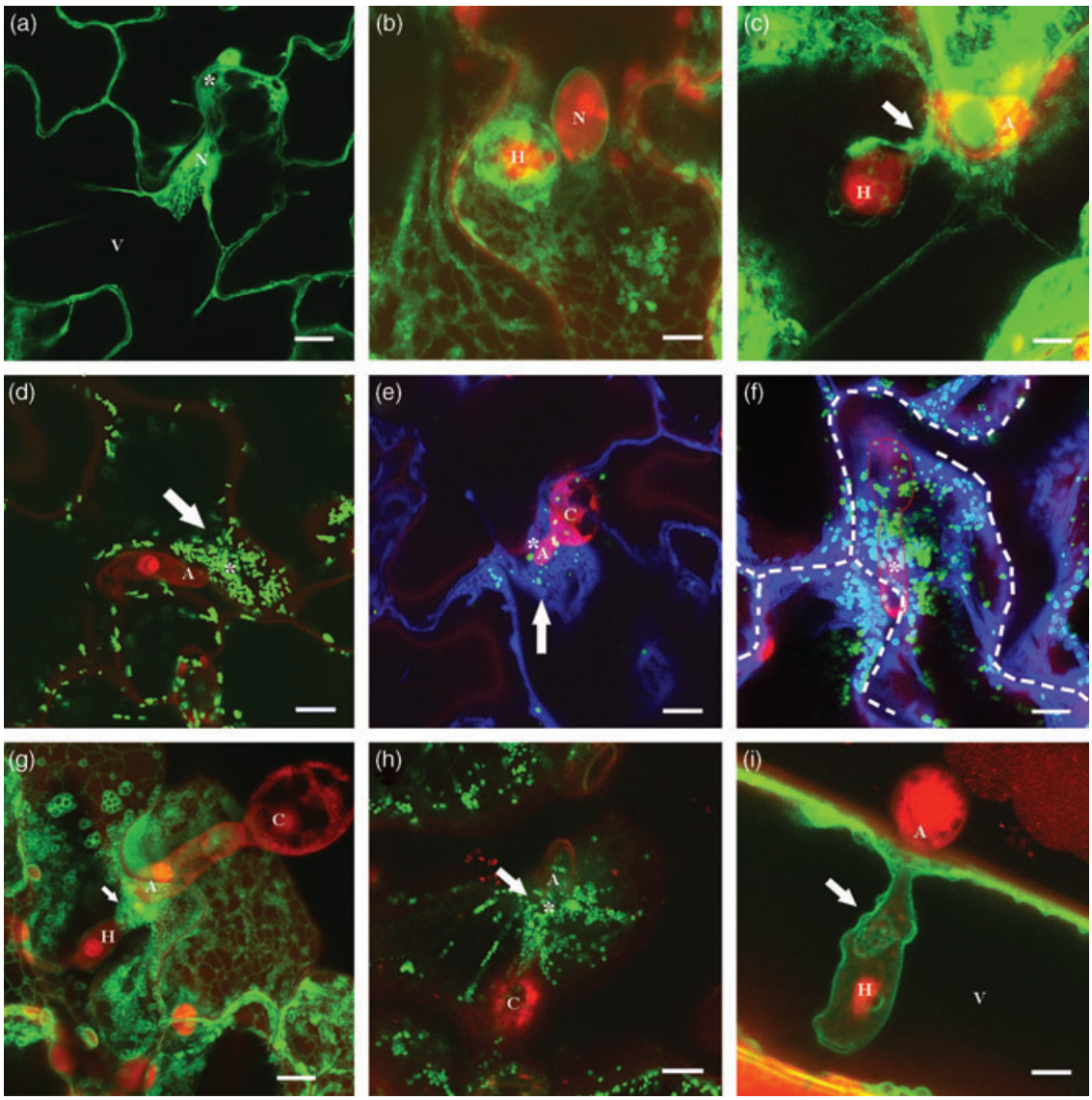

Figure 4. Redistribution of organelles in Arabidopsis epidermal cells under attack by *Erysiphe cichoracearum*.
(a–i) Samples from lines expressing GFP-tagged organelles or subcellular structures (Table 1) were infected with *E. cichoracearum*, stained with propidium iodide (except as noted), then visualized with LSCM. Propidium iodide (red channel) normally stains just fungal structures under these staining conditions, although occasionally the plant cell wall and nucleus will also stain. A, appressorium; C, conidium; H, haustorium; N, nucleus; V, vacuole.
(a) Directional movement of cytoplasm toward a penetration site (*) leading to an aggregation of cytoplasm and organelles in a stage 1 infection. Cytoplasm labeled with soluble GFP (EGAD line). A single time-frame image is shown. Bar = 14.5 μm.
(b) Close contact between nucleus and haustorial complex was observed. The haustorial complex is encompassed by the ER (Q4 marker line). Sample visualized in early stage 4. Z-projection of 17 images (0.5 μm per scan). Bar = 4.5 μm.
(c) The haustorial complex is encapsulated by a net of ER (Q4 marker line). The ER aggregates most strongly at the neck of the haustorial complex (arrow). Image taken in early stage 4. Z-projection of 25 images (0.5 μm per scan). Bar = 6 μm.
(d) Overlapped time-lapsed images collected every 5 sec for 5 min showing the aggregation of GFP-labeled peroxisomes (150698l marker line, arrow) adjacent to the infection site (*) at stage 1. Bar = 11 μm.
(e) Accumulation of both YFP-labeled peroxisomes and CFP-labeled cytoplasm at infection sites (*) at early stage 1 (A5Y + ECAD double marker line). FM 4–64 was used to stain fungal structures. A single time-frame image is shown. Bar = 17.8 μm.
(f) Overlapped time-lapsed images collected every 5 sec for 5 min show the aggregation of YFP-tagged peroxisomes and CFP-labeled cytoplasm in the A5Y + ECAD double marker line at the penetration site (*). FM 4–64 was used to stain fungal structures (outlined with red line). Dotted white line shows epidermal cell boundary. Bar = 17.7 μm.
(g) Accumulation of mitochondria (arrow) around the neck of the haustorial complex (*) at stage 3 (Q10 marker line). Z-projection of 40 images (0.5 μm per scan). Bar = 14.5 μm.
(h) Golgi bodies (Dscs line) accumulate (arrow) near the infection site (*) at stage 1. Bar = 7.9 μm. Overlapped time-lapsed images collected every 5 sec for 5 min.
(i) The tonoplast (arrow) closely surrounds the haustorial complex (Q5 marker line). Z-projection of 17 images (0.5 μm per scan). Bar = 4.0 μm.

aggregated underneath appressoria by stage 1. Long-distance movement of peroxisomes towards penetration sites slowed in later stages, and peroxisomes that had accumulated in the neck area of the haustorial complex remained localized in this region. The peroxisomes that had aggregated at penetration sites exhibited erratic and short-distance movements (data not shown).

Aggregations of mitochondria and Golgi bodies around the haustorial complex neck region were also observed (Figure 4g,h), and their behavior was very similar to that of the peroxisomes. Although organelles occurred at high density adjacent to the haustorial complex, none of the GFP-tagged marker proteins appeared in the EHM, suggesting there was no transfer of markers between organelles and EHM.

One possibility suggested by the accumulation of organelles and cytoplasm at penetration sites was that they were carried together. A prediction from this hypothesis is that the density of organelles per unit of cytoplasm would be similar at sites near and distal to penetration sites. The numbers of peroxisomes and amount of cytoplasm were quantified in four concentric zones emanating from a penetration site in a double marker line with YFP-tagged peroxisomes (A5Y) and soluble CFP in the cytoplasm as a means of testing this prediction (Figure 5). The distribution of cytoplasm was highest closest to penetration sites, and decreased with increasing distance from penetration sites (Table 3). Similarly, the occurrence of peroxisomes nearest penetration sites was roughly twice that at more distal sites (Table 3). However, the density of peroxisomes was also higher at penetration sites, suggesting preferential accumulation of this organelle relative to cytoplasm.

Vacuole. The Arabidopsis epidermal cell is filled with a large central vacuole, as well as with small vacuoles. The vacuoles were variable in size and shape due to cytoplasmic streaming and vesicle fusions, as shown by the Q5 line (Figure 4i). In an infected cell the haustorial complex was closely surrounded by the tonoplast (Figure 4i). TEM images from previous studies show that the EHM is a separate membrane from the tonoplast (Bracker, 1968; Dahmen and Hobot, 1986; Hippe-Sanwald, 1995; Hippe-Sanwald *et al.*, 1992; McKeen, 1974). In addition, in the Q5Y + ECAD double marker line a thin layer of cytoplasm separated the tonoplast from the haustorial complex, showing that the tonoplast is a separate membrane from the EHM, and that the EHM does not contain the YFP-Q5 marker (Figure S1).

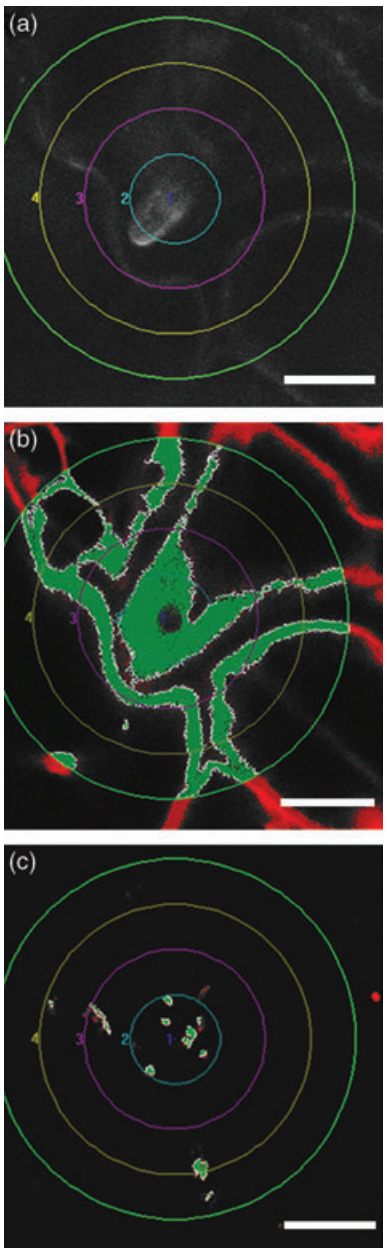

Figure 5. Cytoplasm and peroxisome aggregation at penetration sites.
The double marker line A5Y + ECAD was infected with *Erysiphe cichoracearum*. ECFP was used to label the host cytoplasm and YFP-A5 to label peroxisomes. Fungal structures were stained with FM 4-64.
(a) Four zones, centered on a penetration site, were created showing the aggregation of cytoplasm (labeled with CFP) at a penetration site.
(b) Cytoplasm (labeled with CFP) that exceeds the signal intensity threshold within the measurement zones is shown in green; that outside the measurement zones in red.
(c) Distribution of YFP-tagged peroxisomes in each of the four measurement zones in an infected epidermal cell.

Discussion

In this study, live-cell LSCM with various organellar GFP marker lines was used to visualize early responses of Arabidopsis cells to infection by the compatible powdery mildew *E. cichoracearum* UCSC1. In addition to allowing us to observe the dynamic responses of plant cells to this biotic

Table 3 Cytoplasmic and peroxisome aggregation at penetration sites

Zone	Proportion of cytoplasm[a]	Peroxisomes[b]
1	0.782 ± 0.165 (1)[c]	0.046 ± 0.021 (1)[c]
2	0.404 ± 0.136 (2)	0.021 ± 0.010 (2)
3	0.210 ± 0.138 (3)	0.025 ± 0.015 (2)
4	0.140 ± 0.108 (3)	0.020 ± 0.021 (2)

[a]Proportion of area in zone occupied by cytoplasm. Zones were centered on a fungal penetration site, with zone 1 closest to the penetration site. See Figure 5 for a description of each zone.
[b]Number of peroxisomes per μm^2 cytoplasm.
[c]Measurements were made on five epidermal cells infected by *Erysiphe cichoracearum*. Means and standard deviations are shown. Data were analyzed by two-way ANOVA, giving values of $P = 1.26^{-06}$ (cytoplasm per zone) and $P = 0.027$ (peroxisomes per area of cytoplasm) for the parameter zone. Values within a column followed by the same number in parentheses do not differ significantly from each other by Fisher's least significant difference test ($P = 0.05$).

stress, these GFP marker lines also provided information about the formation of the EHM, the membrane interface between plant cytoplasm and the fungal haustorium.

The EHM has often been considered an invaginated extension of the plant plasma membrane. However, some cytological and biochemical studies have shown that, although the EHM shares some epitopes in common with the plasma membrane, several of its properties and biochemical markers differ from the plasma membrane (Bracker, 1968; Bushnell and Gay, 1978; Green *et al.*, 1995; Manners and Gay, 1983; Spencer-Phillips and Gay, 1981). In this study, none of eight plasma membrane GFP markers occurred in the EHM. Instead, the plasma membrane appeared to terminate in a collar-like structure at the neck of haustorial complexes (Figure 2). This GFP-labeled collar looked like a folded sheath adjacent to fungal penetration pegs (Figure 2k). The haustorial neckband may serve as a barrier separating the plasma membrane from the EHM, limiting the exchange of components between these two membranes (Bracker, 1968; Ebrahim-Nesbat *et al.*, 1983; Edwards and Allen, 1970; Heath and Škalamera, 1997). These data from live *in vivo* imaging strongly support the idea that the EHM is not just a simple extension of plasma membrane.

How then is the EHM formed? We formulated two working models of EHM formation during haustorial complex development (Figure 6). The first hypothesis suggests that the EHM results from invagination and differentiation of the host plasma membrane during haustorium development. New plasma membrane is added throughout the cell, and not to the EHM directly, due to rapid vesicle fusion (Figure 2l). High rates of membrane addition (green vesicles, Figure 6) near the site of penetration result in pouch-like lobes of plasma membrane (Figure 2c–e). The EHM forms by invagination of the plasma membrane as a consequence of fungal penetration. The haustorial neckband might selectively sieve proteins from the invaginating membrane at an early penetration stage, differentiating the protein composition of the EHM from the plasma membrane. The second hypothesis is that the EHM is built *de novo* by targeted secretion of specialized vesicles (purple vesicles, Figure 6) with EHM-specific components from the earliest stages of

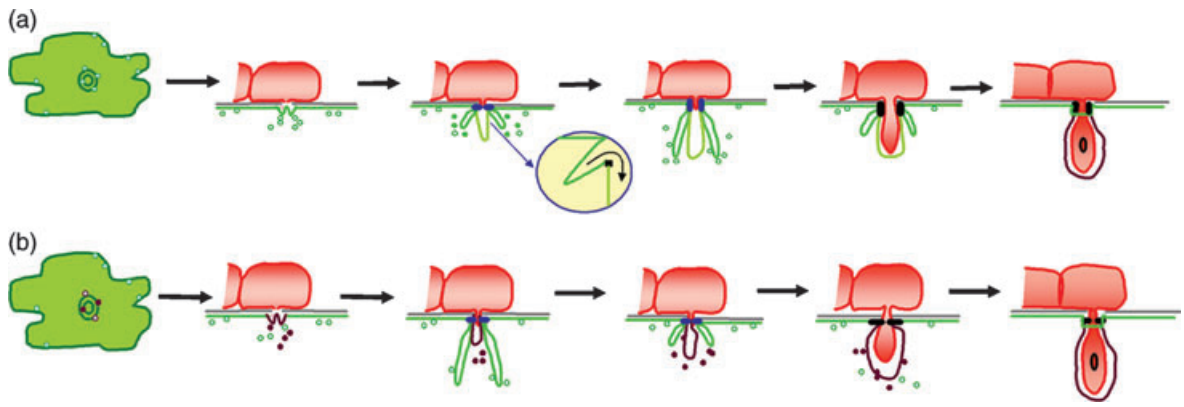

Figure 6. Two alternative hypotheses to explain the formation of the extrahaustorial membrane (EHM).
(a) Hypothesis 1: the EHM forms by invagination and differentiation of the host plasma membrane during haustorial complex development. New plasma membrane is synthesized throughout the cell. High rates of membrane addition (green vesicles) near the site of penetration result in lobes or pouches of excess plasma membrane at sites where the haustorial complex will develop. Invagination of the plasma membrane by fungal penetration is accompanied by rapid differentiation of the membrane. The haustorial neckband may selectively sieve proteins from the invaginating membrane, removing many plasma membrane proteins from the developing EHM.
(b) Hypothesis 2: the EHM is formed *de novo* by targeted secretion of specialized EHM-specific vesicles (purple) from the earliest stages of fungal penetration. Relocated nucleus, ER and Golgi bodies near the haustorial complex and rapid vesicular fusion at the penetration site could support new membrane synthesis for the EHM.
In both hypotheses, additional editing of the new EHM by both fungus and host may be involved in producing a mature, functional EHM.

fungal penetration. In both models, modification of the EHM by both host and pathogen could continue until the EHM is mature, as suggested by studies with stage-specific monoclonal antibodies (Green *et al.*, 1995; Mackie *et al.*, 1993; Roberts *et al.*, 1993). Studies of the method by which the EHM is formed and acquires its distinct functional properties await the availability of EHM-specific markers and purification methods that allow separation of the EHM from other host membranes.

Recently, Felle *et al.* (2004) reported that changes in apoplastic H^+ and Ca^{2+} concentrations occurred at about 2 and 10 hai during compatible powdery mildew infections of barley. The timing of the first changes in pH and Ca^{2+} concentration may cue the plant cell to prime its surveillance system to further disturbance. One of the earliest responses to fungal penetration attempts was the formation of rings (Figure 2i). These rings could be physical evidence for the alarmed state of the cell prior to actual penetration events. The coincidence between the diameter of the rings and of papillae, and the observation that both rings and papillae can cross cell-wall boundaries into adjacent cells, suggest that these two structures are associated in some manner. Cytoplasmic aggregates, visualized by Nomarski microscopy, may also be associated with the formation of the rings and with papillae (Bushnell and Bergquist, 1975; Bushnell and Zeyen, 1976). The later changes in apoplastic Ca^{2+} concentration and pH correlated with the appearance of papillae and are consistent with an influx of Ca^{2+} from the apoplast to the cytoplasm to activate callose synthase, which synthesizes callose, a major constituent of papillae (Bolwell *et al.*, 2002; Felle *et al.*, 2004; Kartusch, 2003).

The observation that these rings form across cell-wall boundaries suggests that a diffusible elicitor in the apoplastic space triggers the formation of these structures. The conidial exudates released within minutes of contact with a leaf surface may provide such an elicitor (Nicholson *et al.*, 1988; Pascholati *et al.*, 1992). However, one might predict that a diffusible signal emanating from the penetration site would stimulate the formation of a disk-like aggregation of protein with the highest concentration of protein adjacent to the penetration site. Some additional factor must be required to limit the accumulation of protein to discrete rings.

Previous work described the accumulation of cytoplasmic aggregates at penetration sites (Bushnell and Zeyen, 1976; Kobayashi *et al.*, 1995). In this work, we similarly observed the accumulation of cytoplasm and organelles at penetration sites, near haustorial necks (Figures 4 and 5). Takemoto *et al.* (2003) observed that ER and Golgi accumulate at the base of downy mildew haustorial complexes rather than at the neck region. The significance of this difference in endomembrane accumulation adjacent to haustorial complexes between the two pathogens is unclear. Our quantitative analysis of the accumulation of peroxisomes and cytoplasm at penetration sites suggests that peroxisomes accumulate preferentially at penetration sites. This fact suggests that peroxisomes are not simply carried with the cytoplasm, but some mechanism specifically facilitates their aggregation at penetration sites. Similar quantitative studies of the aggregation of other organelles at penetration sites would suggest whether peroxisomes are the only organelles to accumulate preferentially, or whether this preferential aggregation is a general subcellular response to fungal attack.

The aggregation of organelles in the haustorial neck region may serve several purposes in the interaction between host and pathogen. Cell-wall materials, to seal the breach in the cell wall created by the pathogen and to reinforce the plant cell wall, and some defense compounds (e.g. pathogenesis-related proteins, phytoalexins) are delivered to the apoplast largely by vesicle trafficking (Bushnell and Zeyen, 1976). Consistent with this idea, *PEN1* and its barley homolog *ROR2* encode syntaxins that accumulate in the plasma membrane at penetration sites and appear to play a role in deposition of papillae and basal disease resistance (Assaad *et al.*, 2004; Bhat *et al.*, 2005; Collins *et al.*, 2003). The function of peroxisomes in the epidermis is largely unknown, but they may participate in degrading reactive oxygen species generated at penetration sites to limit the extent of damage from these molecules, particularly in compatible interactions. The identification of vesicle trafficking components, in addition to PEN1, and of cytoskeletal elements specialized for plant–pathogen interactions would advance our understanding of these early subcellular responses to infection and how they differ between compatible and incompatible interactions.

Experimental procedures

Plant and fungal materials

Arabidopsis thaliana (Col-0) seeds of lines carrying GFP-tagged organelle markers were developed by D.E. and Sean Cutler (http://deepgreen.stanford.edu/) (Cutler *et al.*, 2000). YFP versions of some markers were created by D.E. and R. Kamyar, Carnegie Institution (unpublished). Double marker lines, A5Y + ECAD and Q5Y + ECAD, were newly generated in this study by genetic crossing. The list of single or double marker lines used in this study is presented in Table 1. Seeds were disinfested with 95% ethanol, rinsed with sterile water and air-dried. Seeds were then mixed with 0.15% agar (Research Organics, Cleveland, OH, USA) and planted on nutrient agar plates [MS salts 4.3 g l^{-1} pH 5.7, 1.5% agar (Sigma, St Louis, MO, USA)]. Germinating seeds were cold-treated at 4°C for 2 days and then placed in a growth chamber (14 h light/10 h dark, 22°C, 100–150 μE m^{-2} sec^{-1} in the 400- to 700-nm range). Five to seven days post-germination, plants were screened for GFP expression using a MZ12 dissecting microscope (Leica Microsystems Inc., Exton, PA, USA) equipped with a mercury lamp and the epifluorescence filter set specifically designed for viewing GFP in plant tissues. Plants expressing GFP were then transferred to soil and placed in a

growth chamber with growth conditions as above. CFP seedlings were selected using the LSCM (Bio-Rad MRC 1024, Hercules, CA, USA) with an He/Cd laser (422 nm excitation).

The powdery mildew fungus *Erysiphe cichoracearum* UCSC1 was maintained on compatible squash plants, variety Kuta (Park Seed, Greenwood, SC, USA) in a growth chamber with the same light cycle as above (Wilson *et al.*, 2001). The inoculum was prepared by touching uninfected squash leaves with previously infected squash leaves 8–10 days before use in Arabidopsis inoculations (Adam *et al.*, 1999).

Light microscopy

Arabidopsis seedlings 2–3 weeks old were infected by shaking *E. cichoracearum*-infected squash leaves over pots containing the seedlings. The pots were placed in a high-humidity chamber for 1 h, then moved to growth chambers (14 h light/10 h dark, 22°C). Infected true leaves (leaf 3 or 4) were then examined at different time points after inoculation using a Leica stereoscope, after staining the leaves with trypan blue solution [0.01% trypan blue (v/v) in lactic acid:H_2O:glacial acetic acid (1:1:1)] (Adam and Somerville, 1996). Images were captured using a Leica DC500 camera and processed using Adobe PHOTOSHOP 7.0 (Adobe Systems Inc., San Jose, CA, USA).

Laser scanning confocal microscopy

Arabidopsis seedlings 2–3 weeks old were inoculated as described above. Infected leaves were then examined at different time points after inoculation by staining leaves in either propidium iodide solution [0.5% propidium iodide (Sigma), 0.01% Silwet (Lehle Seeds, Round Rock, TX, USA), 2.5% mannitol (Sigma) in water] or FM 4–64 solution [10 μg ml^{-1} FM 4–64 (Molecular Probes, Eugene, OR, USA), 0.01% Silwet, 2.5% mannitol in water] to visualize the fungal structures. Haustorial complexes in the epidermal cells were observed on a Nikon Diaphot 200 inverted fluorescence microscope equipped with Nikon 60 × 1.2 numerical aperture water immersion objective and a Bio-Rad MRC 1024 confocal head. The samples were excited with two lasers (Ar/Kr and He/Cd) at the following wavelengths: 442 nm (CFP); 488 nm [FM 1–43 (Molecular Probes), GFP and YFP]; 568 nm (propidium iodide and FM 4–64). Collected image data sets were subsequently analyzed with the digital image analyzing programs IMAGEJ ver. 1.30 (http://rsb.info.nih.gov/ij); CAS40 (CONFOCAL ASSISTANT ver. 4.02, http://www.cyto.purdue.edu/flowcyt/software/cas402.htm); VOLOCITY (Improvision Inc., Lexington, MA, USA); and Adobe PHOTOSHOP 7.0.

Detection of callose in papillae was done with an anti-callose monoclonal antibody (Biosupplies Australia Pty Ltd, Parkville, Australia) followed by a secondary antibody labeled with Alexa 488 (Molecular Probes) (Nishimura *et al.*, 2003).

For the data presented in Figure 5 and Table 3, peroxisome number and cytoplasm content were measured from single confocal sections in defined regions emanating from penetration sites by METAMORPH ver. 4.3 (Sydney, Australia). To do this, four annulus-shaped zones centered on a penetration site were created. The innermost zone (zone 1) was a circle with a diameter of 13 μm (area, 132.7 μm^2). Zone 2 was an annulus 13–26 μm in diameter (area, 398.0 μm^2); zone 3 an annulus 26–39 μm in diameter (area, 663.3 μm^2); and zone 4 an annulus 39–52 μm in diameter (area, 928.7 μm^2). A threshold signal intensity for the fluorescence from ECAD was set when determining the proportion of the area of each zone occupied by cytoplasm. The A5 marker protein tagged with YFP was used to mark peroxisomes, and the number of peroxisomes per zone was counted.

Transmission electron microscopy

Arabidopsis seedlings 2–3 weeks old were inoculated as described above. At 24 hai, infected leaves were cut and fixed in 3% glutaraldehyde for 2 h. Fixed tissues were rinsed in 0.05 M potassium phosphate buffer (pH 6.8) and post-fixed in 2% OsO_4 for 2 h. After rinsing in 0.05 M potassium phosphate buffer (pH 6.8), samples were dehydrated in series of ethanol and embedded in Spurr's resin (Electron Microscopic Sciences, Fort Washington, PA, USA). Thin sections were stained in 2% uranyl acetate (pH 5.0) followed by 0.01 M lead citrate (pH 12), and viewed with a Philips 201 transmission electron microscope (Nishimura *et al.*, 2003).

Isolation of haustorial complexes

Intact haustorial complexes were isolated according to the protocol of Gil and Gay (1977) from *E. cichoracearum*-infected Kuta squash leaves. Isolated haustorial complexes were stained with FM 1–43 solution (as described above for the dye FM 4–64) or propidium iodide and visualized by LSCM. Collected Z-series image data sets were subsequently transferred to the digital image analyzing program VOLOCITY for 3D volume rendering.

Acknowledgements

We thank Roheena Kamyar (Carnegie Institution) for creating YFP versions of the marker lines and Joan Chory (Salk Institute) for sharing Bri1-GFP seeds. We also thank Matt Humphry and Monica Stein (Carnegie Institution) for many helpful suggestions. This work is supported in part by the Carnegie Institution and the National Science Foundation.

Supplementary Material

The following supplementary material is available for this article online:

Figure S1. A thin layer of cytoplasm separates the tonoplast from the haustorial complex.

This material is available as part of the online article from http://www.blackwell-synergy.com

References

Adam, L. and Somerville, S.C. (1996) Genetic characterization of five powdery mildew disease resistance loci in *Arabidopsis thaliana*. *Plant J.* **9**, 341–356.

Adam, L., Ellwood, S., Wilson, I., Saenz, G., Xiao, S., Oliver, R.P., Turner, J.G. and Somerville, S. (1999) Comparison of *Erysiphe cichoracearum* and *E. cruciferarum* and a survey of 360 *Arabidopsis thaliana* accessions for resistance to these two powdery mildew pathogens. *Mol. Plant Microbe Interact.* **12**, 1031–1043.

Agrios, G.N. (1997) *Plant Pathology*, 4th edn. San Diego, CA, USA: Academic Press.

Assaad, F., Qiu, J.-L., Youngs, H. *et al.* (2004) The PEN1 syntaxin defines a novel cellular compartment upon fungal attack and is required for the timely assembly of papillae. *Mol. Biol. Cell*, **15**, 5118–5129.

Baluška, F., Bacigalova, K., Oud, J.L., Hauskrecht, M. and Kubica, S. (1995) Rapid reorganization of microtubular cytoskeleton

accompanies early changes in nuclear ploidy and chromatin structure in postmitotic cells of barley leaves infected with powdery mildew. *Protoplasma*, **185**, 140–151.

Bhat, R.A., Miklis, M., Schmelzer, E., Schulze-Lefert, P. and Panstruga, R. (2005) Recruitment and interaction dynamics of plant penetration resistance components in a plasma membrane microdomain. *Proc. Natl Acad. Sci. USA*, **102**, 3135–3140.

Bolwell, G.P., Bindschedler, L.V., Blee, K.A., Butt, V.S., Davies, D.R., Gardner, S.L., Gerrish, C. and Minibayeva, F. (2002) The apoplastic oxidative burst in response to biotic stress in plants: a three-component system. *J. Exp. Bot.* **372**, 1367–1376.

Bracker, C.E. (1968) Ultrastructure of the haustorial apparatus of *Erysiphe graminis* and its relationship to the epidermal cell of barley. *Phytopathology*, **58**, 12–30.

Braun, U. (1987) *A Monograph of the Erysiphales (Powdery Mildews). Beihefte zür Hova Hewigia, Helft 89*. Berlin: J. Cramer.

Bushnell, W.R. (1972) Physiology of fungal haustoria. *Annu. Rev. Phytopathol.* **10**, 151–176.

Bushnell, W.R. (2002) The role of powdery mildew research in understanding host–parasite interaction: past, present and future. In *The Powdery Mildews, A Comprehensive Treatise* (Belanger, R.R., Bushnell, W.R., Dik, A.J. and Carver, T.L.W., eds). St Paul, MN, USA: APS Press, pp. 1–12.

Bushnell, W.R. and Bergquist, S.E. (1975) Aggregation of host cytoplasm and the formation of papillae and haustoria in powdery mildew of barley. *Phytopathology*, **65**, 310–318.

Bushnell, W.R. and Gay, J.L. (1978) Accumulation of solutes in relation to the structure and function of haustoria in powdery mildews. In *The Powdery Mildews* (Spencer, D.M., ed.). London: Academic Press, pp. 183–235.

Bushnell, W.R. and Zeyen, R.J. (1976) Light and electron microscope studies of cytoplasmic aggregates formed in barley cells in response to *Erysiphe graminis*. *Can. J. Bot.* **54**, 1647–1655.

Clark, T.A., Zeyen, R.J., Carver, T.L.W., Smith, A.G. and Bushnell, W.R. (1995) Epidermal cell cytoplasmic events and response gene transcript accumulation during *Erysiphe graminis* attack in isogenic barley lines differing at the *Ml-o* locus. *Physiol. Mol. Plant Pathol.* **46**, 1–16.

Collins, N.C., Thordal-Christensen, H., Lipka, V. *et al.* (2003) SNARE-protein-mediated disease resistance in the plant cell wall. *Nature*, **425**, 973–977.

Cutler, S.R., Ehrhardt, D.W., Griffitts, J.S. and Somerville, C.R. (2000) Random GFP:cDNA fusions enable visualization of subcellular structures in cells of Arabidopsis at a high frequency. *Proc. Natl Acad. Sci. USA*, **97**, 3718–3723.

Dahmen, H. and Hobot, J.A. (1986) Ultrastructural analysis of *Erysiphe graminis* haustoria and subcuticular stroma of *Venturia inaequalis* using cryosubstitution. *Protoplasma*, **131**, 92–102.

Ebrahim-Nesbat, F., Balder, H. and Schönbeck, F. (1983) Elektronenmikroskopische untersuchungen des gerstenmehltaus (*Erysiphe graminis* DC f. sp. *hordei* Marchal) nach resistenzinduktion mit mikrobiellen stoffwechselprodukten. *Phytopathol. Z.* **106**, 76–89.

Edwards, H.H. and Allen, P.J. (1970) A fine-structure study of the primary infection process during infection of barley by *Erysiphe graminis* f. sp. *hordei*. *Phytopathology*, **60**, 1504–1509.

Ehrhardt, D. (2003) GFP technology for live cell imaging. *Curr. Opin. Plant Biol.* **6**, 622–628.

Felle, H.H., Herrmann, A., Hanstein, S., Hückelhoven, R. and Kogel, K.-H. (2004) Apoplastic pH signaling in barley leaves attacked by the powdery mildew fungus *Blumeria graminis* f. sp. *hordei*. *Mol. Plant Microbe Interact.* **17**, 118–123.

Friedrichsen, D.M., Joazeiro, C.A.P., Li, J.M., Hunter, T. and Chory, J. (2000) Brassinosteroid-insenstive-1 is a ubiquitously expressed leucine-rich repeat receptor serine/threonine kinase. *Plant Physiol.* **123**, 1247–1255.

Gil, F. and Gay, J.L. (1977) Ultrastructural and physiological properties of the host interfacial components of the haustoria of *Erysiphe pisi in vivo* and *in vitro*. *Physiol. Plant Pathol.* **10**, 1–12.

Green, J.R., Pain, N.A., Cannel, M.E., Jones, G.L., Leckie, C.P., McCready, S., Mendgen, K., Mitchell, A.J., Callow, J.A. and O'Connel, R.J. (1995) Analysis of differentiation and development of the specialized infection structures formed by biotrophic fungal plant pathogens using monoclonal antibodies. *Can. J. Bot.* **73**, S408–S417.

Green, J.R., Carver, T.L.W. and Gurr, S.J. (2002) The formation and function of infection and feeding structures. In *The Powdery Mildews, A Comprehensive Treatise* (Belanger, R.R., Bushnell, W.R., Dik, A.J. and Carver, T.L.W., eds). St Paul, MN, USA: APS Press, pp. 66–82.

Hahn, M., Neef, U., Struck, C., Göttfert, M. and Mendgen, K. (1997) A putative amino acid transporter is specifically expressed in haustoria of the rust fungus *Uromyces fabae*. *Mol. Plant Microbe Interact.* **10**, 438–445.

Heath, M.C. and Škalamera, D. (1997) Cellular interactions between plants and biotrophic fungal parasites. *Adv. Bot. Res.* **24**, 195–225.

Hippe-Sanwald, S. (1995) Low temperature techniques as a tool in plant pathology. *Scan. Microsc.* **9**, 881–899.

Hippe-Sanwald, S., Hermanns, M. and Somerville, S.C. (1992) Ultrastructural comparison of incompatible and compatible interactions in the barley powdery mildew disease. *Protoplasma*, **168**, 27–40.

Kartusch, R. (2003) On the mechanism of callose synthesis induction by metal ions in onion epidermal cells. *Protoplasma*, **220**, 219–225.

Kobayashi, I., Murdoch, L.J., Kunoh, H. and Hardham, A.R. (1995) Cell biology of early events in the plant resistance response to infection by pathogenic fungi. *Can. J. Bot.* **73**, S418–S425.

Koga, H., Bushnell, W.R. and Zeyen, R.J. (1990) Specificity of cell type and timing of events associated with papilla formation and the hypersensitive reaction in leaves of *Hordeum vulgare* attacked by *Erysiphe graminis* f. sp. *hordei*. *Can. J. Bot.* **68**, 2344–2352.

Mackie, A.J., Roberts, A.M., Green, J.R. and Callow, J.A. (1993) Glycoproteins recognized by monoclonal antibodies UB7, UB8, and UB10 are expressed early in the development of pea powdery mildew haustoria. *Physiol. Mol. Plant Pathol.* **43**, 135–146.

Manners, J.M. and Gay, J.L. (1977) The morphology of haustorial complexes isolated from apple, barley, beet and vine infected with powdery mildews. *Physiol. Plant Pathol.* **11**, 261–266.

Manners, J.M. and Gay, J.L. (1982) Transport, translocation and metabolism of ^{14}C-photosynthates at the host–parasite interface of *Pisum sativum* and *Erysiphe pisi*. *New Phytol.* **92**, 221–244.

Manners, J.M. and Gay, J.L. (1983) The host–parasite interface and nutrient transfer in biotrophic parasitism. In *Biochemical Plant Pathology* (Callow, J.A., ed.). New York: John Wiley & Sons, pp. 163–195.

McKeen, W.E. (1974) The interface between the powdery mildew haustorium and the cytoplasm of the susceptible barley epidermal cell. *Can. J. Microbiol.* **20**, 1475–1478.

Mendgen, K., Bachem, U., Stark-Urnau, M. and Xu, H. (1995) Secretion and endocytosis at the interface of plants and fungi. *Can. J. Bot.* **73**, S640–S648.

Miyawaki, A., Llopis, J., Heim, R., McCaffery, J.M., Adams, J.A., Ikura, M. and Tsien, R.Y. (1997) Fluorescent indicators for Ca^{2+} based on green fluorescent proteins and calmodulin. *Nature*, **388**, 882–887.

Nicholson, R.L. and Kunoh, H. (1994) Early interactions, adhesion, and establishment of the infection court by *Erysiphe graminis*. *Can. J. Bot.* **73**, S609–S615.

Nicholson, R.L., Yoshioka, H., Yamaoka, N. and Kunoh, H. (1988) Preparation of the infection court by *Erysiphe graminis*. II. Release of esterase enzyme from conidia in response to a contact stimulus. *Exp. Mycol.* **12**, 336–349.

Nishimura, M.T., Stein, M., Hou, B.-H., Vogel, J.P., Edwards, H. and Somerville, S.C. (2003) Loss of a callose synthase results in salicylic acid-dependent disease resistance. *Science*, **301**, 969–972.

Pascholati, S.F., Yoshioka, H., Kunoh, H. and Nicholson, R.L. (1992) Preparation of the infection court by *Erysiphe graminis* f. sp. *hordei*: cutinase is a component of the conidial exudates. *Physiol. Mol. Plant Pathol.* **41**, 53–59.

Plotnikova, J.M., Reuber, T.L., Ausubel, F.M. and Pfister, D.H. (1998) Powdery mildew pathogenesis of *Arabidopsis thaliana*. *Mycologia*, **90**, 1009–1016.

Roberts, A.M., Mackie, A.J., Hathaway, V., Callow, J.A. and Green, J.R. (1993) Molecular differentiation in the extrahaustorial membrane of pea powdery mildew haustoria at early and late stages of development. *Physiol. Mol. Plant Pathol.* **43**, 147–160.

Škalamera, D. and Heath, M.C. (1998) Changes in the cytoskeleton accompanying infection induced nuclear movements and the hypersensitive response in plant cells invaded by rust fungi. *Plant J.* **16**, 191–200.

Spencer-Phillips, P.T.N. and Gay, J.L. (1981) Plasma membrane ATPase domains and transport through infected cells. *New Phytol.* **89**, 393–400.

Sutton, P.N., Henry, M.J. and Hall, J.L. (1999) Glucose, and not sucrose, is transported from wheat to wheat powdery mildew. *Planta*, **208**, 426–430.

Takemoto, D., Jones, D.A. and Hardham, A.R. (2003) GFP-tagging of cell components reveals the dynamics of subcellular reorganization in response to infection of Arabidopsis by oomycete pathogens. *Plant J.* **33**, 775–792.

Voegele, R.T., Struck, C., Hahn, M. and Mendgen, K. (2001) The role of haustoria in sugar supply during infection of broad bean by the rust fungus *Uromyces fabae*. *Proc. Natl Acad. Sci. USA*, **98**,8133–8138.

Wilson, I.W., Schiff, C.L., Hughes, D.E. and Somerville, S.C. (2001) Quantitative trait loci analysis of powdery mildew disease resistance in the *Arabidopsis thaliana* accession Kashmir-1. *Genetics*, **158**, 1301–1309.

Zeyen, R.J. and Bushnell, W.R. (1979) Papilla response of barley epidermal cells caused by *Erysiphe graminis*: rate and method of deposition determined by microcinematograpy and transmission microscopy. *Can. J. Bot.* **57**, 898–913.

Zeyen, R.J., Carver, T.L.W. and Lyngkjaer, M.F. 2002. Epidermal cell papillae. In *The Powdery Mildews, A Comprehensive Treatise* (Belanger, R.R., Bushnell, W.R., Dik, A.J. and Carver, T.L.W., eds). St Paul, MN, USA: APS Press, pp. 107–125.